



Generalized two-dimensional correlation infrared spectroscopy to reveal mechanisms of CO₂ capture in nitrogen enriched biochar

Xiong Zhang^a, Shihong Zhang^a, Haiping Yang^{a,*}, Jingai Shao^{b,*},
Yingquan Chen^a, Xinjie Liao^a, Xianhua Wang^a, Hanping Chen^{a,b}

^a State Key Laboratory of Coal Combustion, School of Energy and Power Engineering, Huazhong University of Science and Technology, Wuhan 430074, China

^b Department of New Energy Science and Engineering, School of Energy and Power Engineering, Huazhong University of Science and Technology, Wuhan 430074, China

Received 3 December 2015; accepted 9 June 2016

Available online xxx

Abstract

In order to reveal mechanisms of CO₂ adsorption–desorption on the nitrogen enriched biochar, the *in situ* diffuse reflectance infrared Fourier transform spectroscopy (*in situ* DRIFTS) was used to monitor the interfacial reaction between CO₂ and nitrogen enriched biochar, and all spectral data sets of *in situ* DRIFTS was parsed by two-dimensional (2D) perturbation correlation. The results show that when the adsorption temperature is between 30 and 60 °C, the hydroxyl, primary amide, amines, azo compound N=N, secondary amide groups and aliphatic C–N/C–O are all effective active sites to adsorb CO₂; while the temperature rises to 120 °C, the CO₂ adsorption capacity of secondary amide group shows a downward trend. After the adsorption of CO₂, these active sites are mainly converted to C=O groups (such as N–COOH, N–COO[−] and aldehyde groups), nitrogen atom-containing heterocyclic groups (pyridine-like groups), and N–O groups (nitrate). Moreover, at 200 °C, the majority of hydroxyl and secondary amide groups as well as part of primary amide, amines and azo compound N=N can be regenerated, while the aliphatic C–N/C–O groups are difficult to be regenerated.

© 2016 by The Combustion Institute. Published by Elsevier Inc.

Keywords: 2D correlation spectroscopy; *In situ* DRIFTS; CO₂ capture; Nitrogen enriched biochar

1. Introduction

Global warming resulting from an increase in atmospheric level of greenhouse gases, especially

CO₂, has become a critical issue in recent times [1]. Absorption [2], adsorption [3], cryogenic distillation [4] and membrane separation [5] are regarded as the effective methods to capture CO₂. One of them, adsorption, is a promising option for CO₂ separation since it offers a number of advantages: low energy requirement for regeneration and elimination of corrosion problems on amine solution

* Corresponding authors. Fax: +86 27 87545526.

E-mail addresses: yhping2002@163.com (H. Yang), jashao@hust.edu.cn (J. Shao).

<http://dx.doi.org/10.1016/j.proci.2016.06.062>

1540-7489 © 2016 by The Combustion Institute. Published by Elsevier Inc.

[6]. Among all adsorbents, the nitrogen enriched biochars are considered as suitable candidates for CO₂ capture since their wide availability, renewable precursors, low cost, high thermal stability and low sensitivity to moisture [7–12].

The CO₂ adsorption properties of nitrogen enriched biochar depend to a large extent not only on the surface area and pore structure, but also the chemical property [7]. At high temperatures, it has been recognized that the chemical property plays a more important role [9]. Furthermore, it is the main factor that affects the regeneration of nitrogen enriched biochars. The diversity of chemical properties are largely derived from the surface chemical heterogeneity that refers to the non-carbon atoms, such as hydrogen, nitrogen, oxygen, sulfur and phosphorus [13]. The formation of functional groups from these heteroatoms determine the surface acidity and basicity of nitrogen enriched biochars. In general, the oxygen functional groups provide the acidic character [14]. The surface basicity is closely related to the nitrogen functional groups, which provides effective active sites to adsorb CO₂, *i.e.* dipole–dipole, hydrogen bond, covalent bond, etc. [7]. Furthermore, the regeneration performance of these active sites directly influences the cyclic utilization of nitrogen enriched biochars.

Chang et al. [15] used the conventional *in situ* DRIFTS to investigate the CO₂ adsorption of the –NH₂ functional group on a N-doped SBA-15. Their research results showed that the surface amine sites of N-doped SBA-15 were distinctly CO₂ adsorption sites, and CO₂ was found to adsorb on the amine sites in the form of carbonate and bicarbonate. However, there are few reports about the CO₂ adsorption of other nitrogen functional groups by *in situ* DRIFTS, such as amide group, imide group, lactame group, pyrrolic group, and pyridinic group. The main reason is that the conventional *in situ* DRIFTS analysis is in no position to differentiate overlapped bands arising from spectral signals of different origins [16]. For example, different spectral intensity contributions from individual components of a complex mixture, chemical functional groups experiencing different effects from some external field, or inhomogeneous materials comprising multiple phases or regions, may be ignored [17]. The generalized two-dimensional (2D) perturbation correlation spectroscopy is a quantitative comparison of the patterns of spectral intensity variations along the external variable t observed at two different spectral variables, ν_1 and ν_2 , over some finite observation interval between T_{\min} and T_{\max} [18]. It provides a better resolution of significant peaks that can not only effectively decipher overlapped peaks, even if spectral bands are located close to each other, but also allow for the elucidation of simultaneously and sequentially occurring processes [16].

Accordingly, in this work, the *in situ* DRIFTS and generalized 2D perturbation correlation

method are combined to reveal mechanisms of CO₂ adsorption–desorption on the nitrogen enriched biochar. The effective active sites of CO₂ adsorption on the surface of nitrogen enriched biochar are identified, and their characteristics of deactivation and regeneration are also investigated, which may be helpful for developing the adsorbent of CO₂ capture.

2. Materials and methods

2.1. Materials and characteristic analysis

Biochar (labeled as U-Char), derived from soybean straw pyrolysis at 500 °C in N₂ atmosphere, was used as a precursor for the preparation of nitrogen enriched biochar by the modification of high temperature CO₂–ammonia mixture at 700 °C, labeled as CA700 [19].

The Brunauer–Emmett–Teller surface area (S_{BET}), micropore surface area (S_{mic}) and micropore volume (V_{mic}) of U-Char and CA700 were determined by automatic adsorption equipment (ASAP2020, Micromeritics, USA). S_{mic} and V_{mic} were calculated using the Dubinin–Radushkevich (DR) method. The nitrogen contents were measured with a CHNS elementary analyzer (Vario Micro Cube, Germany). X-ray photoelectron spectroscopy (XPS, AXIS-ULTRA DLD-600 W, Kratos, Japan) was used to determine the type and relative content of functional groups on CA700. The C1s electron binding energy related to graphitic carbon was referenced at 284.6 eV for calibration purposes. The data were analyzed using 20% Lorentzian–Gaussian peak fitting program.

2.2. *In situ*-DRIFTS experiment

A Fourier transform infrared spectroscopy (FTIR, VERTEX 70, Bruker, Germany) equipped with a high temperature controllable DRIFTS cell were used to *in situ* record spectra obtained under different reaction conditions. About 30 mg of CA700 was loaded in the DRIFTS cell. Prior to adsorption, CA700 was pretreated in flowing N₂ (100 ml/min) at 30 °C for 30 min to gain IR background spectrum. Adsorption of CO₂ was initiated by a step switch from the N₂ to 20% CO₂ in N₂ (100 ml/min). The reaction temperature was successively increased to 30 °C, 60 °C, 120 °C, and 200 °C, dwelling at each step of temperatures for 30 min to obtain infrared spectrum. The reaction temperature of 200 °C is more conducive to the CO₂ desorption than adsorption, so this condition can be considered as the regeneration process of CA700.

2.3. Theory of 2D infrared spectroscopy

The 2D perturbation correlation method was used to deal with the infrared spectrum of the CO₂

Table 1

Noda's rules for judging the direction and sequence of intensity changes [16].

| $\Psi(v_1, v_2)$ | $\Phi(v_1, v_2)$ | Implications |
|------------------|------------------|--|
| | + | The intensity of the signals at v_1 and v_2 changes in the same direction, <i>i.e.</i> increasing or decreasing together |
| | - | The intensity of the signals at v_1 and v_2 changes in the opposite direction |
| + | + | The change at v_1 mainly precedes the change in the band at v_2 |
| - | + | The change at v_1 mainly follows the change in the band at v_2 |
| + | - | The change at v_1 mainly follows the change in the band at v_2 |
| - | - | The change at v_1 mainly precedes the change in the band at v_2 |

adsorption-desorption on CA700. The change of temperature is considered to be an external variable t , so the dynamic spectrum $\tilde{a}(v, t)$ of this system is defined as [17]

$$\tilde{a}(v, t) = \begin{cases} a(v, t) - \bar{a}(v), & T_{\min} \leq t \leq T_{\max} \\ 0, & \text{otherwise} \end{cases} \quad (1)$$

Where the variable v is the wavenumber in IR, $a(v, t)$ is the perturbation-induced variation of IR spectral intensity during a period of time between T_{\min} and T_{\max} , and the reference spectrum $a(v)$ is defined as

$$\bar{a}(v) = \frac{1}{T_{\max} - T_{\min}} \int_{T_{\min}}^{T_{\max}} a(v, t) dt \quad (2)$$

The 2D correlation spectrum can be expressed as

$$X(v_1, v_2) = \langle \tilde{a}(v_1, t) \times \tilde{a}(v_2, t') \rangle \quad (3)$$

The symbol $\langle \rangle$ denotes for a cross-correlation function designed to compare the dependence patterns of two chosen quantities on t . In order to simplify the mathematical manipulation, $X(v_1, v_2)$ is treated as a complex number function

$$X(v_1, v_2) = \Phi(v_1, v_2) + i\Psi(v_1, v_2) \quad (4)$$

where $\Phi(v_1, v_2)$ is the synchronous correlation map and $\Psi(v_1, v_2)$ is the asynchronous correlation map. The synchronous 2D correlation intensity $\Phi(v_1, v_2)$ represents the overall similarity or coincident

tal trends between two separate intensity variations measured at different spectral variables. The asynchronous 2D correlation intensity $\Psi(v_1, v_2)$, on the other hand, may be regarded as a measure of dissimilarity.

The synchronous correlation map is a symmetric spectrum with a diagonal line ($v_1 = v_2$). The asynchronous correlation map is antisymmetric with the diagonal. The correlation peak on the diagonal, which only appears at the synchronous spectrum, is referred to as autpeak that is always positive and represents the most susceptible vibrations to changes during the external perturbation. The correlation peak in off-diagonal positions, which can appear at both the synchronous and asynchronous spectrum, is cross peak that can be either positive or negative. The cross peak in the synchronous spectrum suggests the possible existence of a coupled or related origin of the spectral intensity variation. The cross peak in the asynchronous spectrum indicates some bands arise from different sources or functional groups in different molecular environments. Most importantly, with the Noda's rules (shown in Table 1), the direction and sequence of the intensity changes can be judged.

3. Results and discussion

3.1. Physical and chemical properties

Textural properties and N elementary analysis results of U-Char and CA700 are shown in Table 2. It can be observed that the S_{mic} of U-Char and CA700 are much larger than their S_{BET} , which indicates that micropore is the main part of their pore structure. After the high temperature CO_2 -ammonia modification, S_{mic} increases from 250.38 m^2/g to 438.57 m^2/g , and nitrogen content from 1.36 wt% to 5.93 wt%. It indicates that the high temperature CO_2 -ammonia modification makes CA700 have more developed microporous structure and abundant nitrogen functional groups.

Typical C1s, N1s and O1s XPS spectra are used to analyze the surface chemical composition of CA700. Its XPS results are shown in Fig. 1, and deconvolution results listed are in Table 3 [20–22]. It can be seen from Fig. 1 and Table 3 that C1s spectrum was deconvoluted into peak C(1), peak C(2), peak C(3), peak C(4) and peak C(5); they respectively represent graphitic

Table 2

Textural properties and N elementary analysis results.

| Samples | N ₂ adsorption | CO ₂ adsorption | | N (wt.%) |
|---------|--|--|---|----------|
| | S_{BET} (m^2/g) | S_{mic} (m^2/g) | V_{mic} (cm^3/g) | |
| U-Char | 0.04 | 250.38 | 0.100 | 1.36 |
| CA700 | 40.79 | 438.57 | 0.176 | 5.93 |

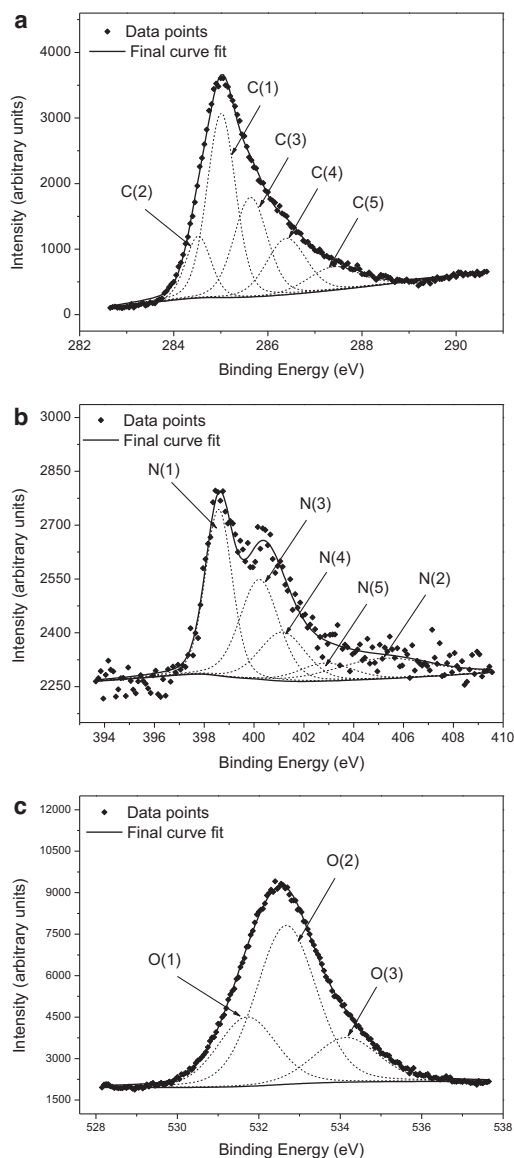


Fig. 1. Typical high resolution XPS spectrum of the C1s (a), N1s (b) and O1s (c) region of CA700.

carbon, carbide carbon, carbon in C=N group, carbon of C–OH and/or C–O–C, and carbon in C=O, quinone and/or C–N group. N1s spectrum was also resolved into five peaks: pyridine-like structures (398.6 eV), chemisorbed nitrogen oxides (405.2 eV), imine/amide/amine/pyrrolic/pyridonic (400.2 eV), quaternary N (401.1 eV) and pyridine-N-oxide/oxidized nitrogen functionalities (402.9 eV). In addition, the amount of pyridine-like structures (32.9 at%) is the highest in all nitrogen functional groups of CA700. O1s spectrum can be deconvoluted into three individ-

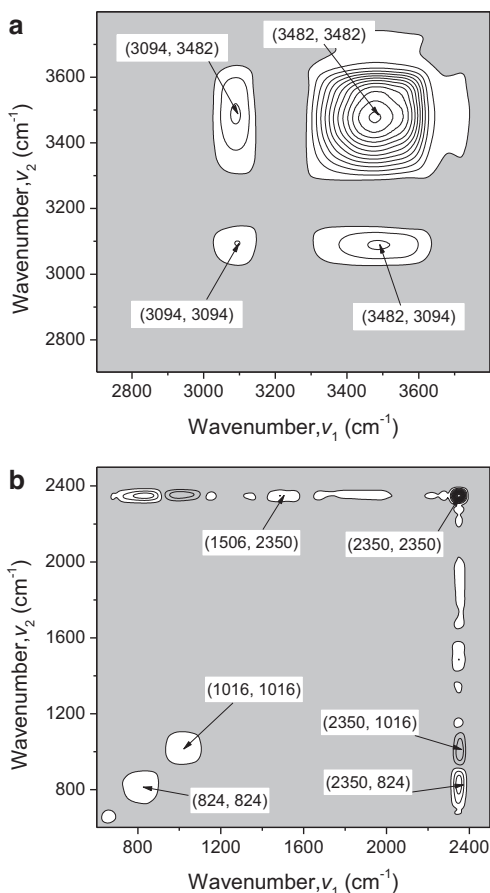


Fig. 2. Synchronous two-dimensional correlation spectrum in 3800–2700 cm^{-1} (a) and 2500–600 cm^{-1} (b). White and gray areas refer to positive and negative intensities, respectively.

ual component peaks, including C=O group in carbonyl/carboxyl/quinone (531.7 eV), C–O group (532.7 eV), Chemisorbed O/water (534.1 eV), and C–O group (57.8 at%) is dominant in these three kinds of oxygen functional groups.

3.2. Synchronous two-dimensional correlation spectrum

Figure 2a and b presents the synchronous correlation maps of two different spectral regions from 3800 cm^{-1} to 2700 cm^{-1} and from 2500 cm^{-1} to 600 cm^{-1} , respectively. Synchronous correlation spectrum in 3800–2700 cm^{-1} shows two strong autopeaks which are $\Phi(3482, 3482)$ and $\Phi(3094, 3094)$, and one positive cross peak at $\Phi(3482, 3094)$. These two autopeaks indicates that primary amide $-\text{NH}_2$ (3482 cm^{-1}) and secondary amide N–H (3094 cm^{-1}) have susceptible changes, responding to the increase of temperature [8]. The

Table 3
Deconvolution results of the C1s, N1s and O1s region.

| Region | Peak | Position (eV) | Assignment | Relative content (at%) |
|--------|------|---------------|---|------------------------|
| C1s | C(1) | 285.0 | Graphite | 38.7 |
| | C(2) | 284.5 | Carbide | 11.5 |
| | C(3) | 285.6 | C=N | 24.6 |
| | C(4) | 286.3 | C–OH, C–O | 16.4 |
| | C(5) | 287.5 | C=O, quinone, C–N | 8.8 |
| N1s | N(1) | 398.6 | Pyridine-like structures | 32.9 |
| | N(2) | 405.2 | Chemisorbed nitrogen oxides | 14.6 |
| | N(3) | 400.2 | Imine, amide, amine, pyrrolic and pyridonic | 28.8 |
| | N(4) | 401.1 | Quaternary N | 16.5 |
| | N(5) | 402.9 | Pyridine-N-oxide, oxidized nitrogen functionalities | 7.2 |
| O1s | O(1) | 531.7 | C=O in carbonyl, carboxyl, quinone | 24.6 |
| | O(2) | 532.7 | C–O, oxygen atoms in hydroxyl groups | 57.8 |
| | O(3) | 534.1 | misorbed O, water | 17.6 |

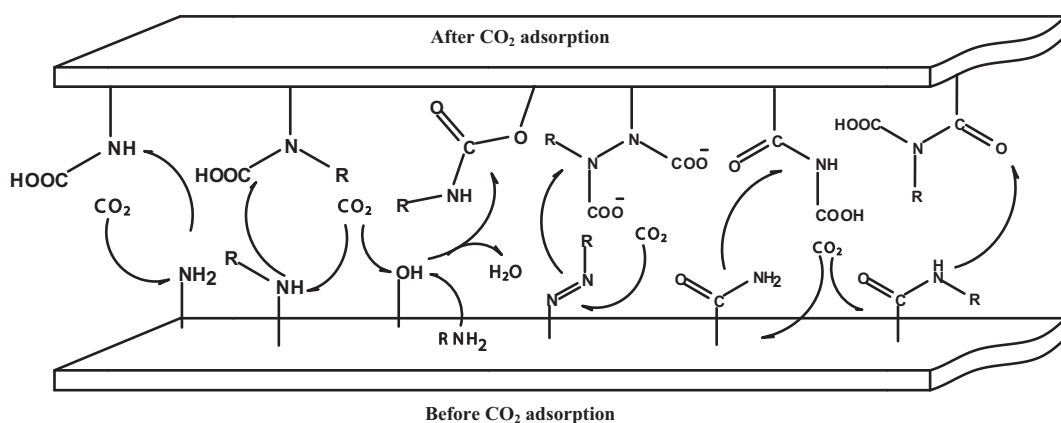


Fig. 3. Mechanisms for the reaction of the nitrogen enriched biochar surface and CO_2 .

synchronous cross peak suggests that the changes of primary amide and secondary amide have the same direction, and both come from the same adsorption mechanism (refer to Fig. 3). In CO_2 atmosphere, the primary amide and secondary amide can react with CO_2 and result in the formation of N–COO [19]. The synchronous correlation maps for $2500\text{--}600\text{ cm}^{-1}$ depicts three strong autopeaks: $\Phi(2350, 2350)$, $\Phi(1016, 1016)$ and $\Phi(824, 824)$, two positive cross peaks: $\Phi(1506, 2350)$ and $\Phi(2350, 824)$, and one negative cross peak: $\Phi(2350, 1016)$. The three strong autopeaks represent that CO_2 (2350 cm^{-1}) on the near-surface of CA700, aliphatic C–N/C–O group (1016 cm^{-1}) and nitrate N–O group (824 cm^{-1}) all intensively respond to the increase of temperature [15,23]. The two positive and one negative synchronous cross peaks confirm that pyridine C=N/C=C group (1506 cm^{-1}), nitrate N–O group and CO_2 on the near-surface have the same direction of change, responding to temperature disturbance, but the change direction of aliphatic C–N/C–O group is the opposite of the three former. These changes are all derived from the

interface reaction between CO_2 and CA700, when the temperature increases.

3.3. Asynchronous two-dimensional correlation spectrum

Figure 4a depicts asynchronous two-dimensional correlation spectrum in $3800\text{--}2700\text{ cm}^{-1}$. There are four couples of asynchronous cross peaks marked in the asynchronous correlation map: $\Psi(3482, 3620)$, $\Psi(3094, 3446)$, $\Psi(3482, 3300)$ and $\Psi(3446, 2891)$, and their values are negative, positive, negative and negative, respectively. These four couples of asynchronous cross peaks indicates that not only primary amide –NH_2 (3482 cm^{-1}) and secondary amide N–H (3094 cm^{-1}) in synchronous correlation map, but also –OH (3620 cm^{-1}), amines (3446 cm^{-1}), pyrrole (3300 cm^{-1}) and aldehyde (2891 cm^{-1}) all response to the increase of temperature [9,10,19]. Furthermore, the synchronous correlation intensities at the same coordinate of the four asynchronous cross peaks are positive $\Phi(3482, 3620)$, positive $\Phi(3094,$

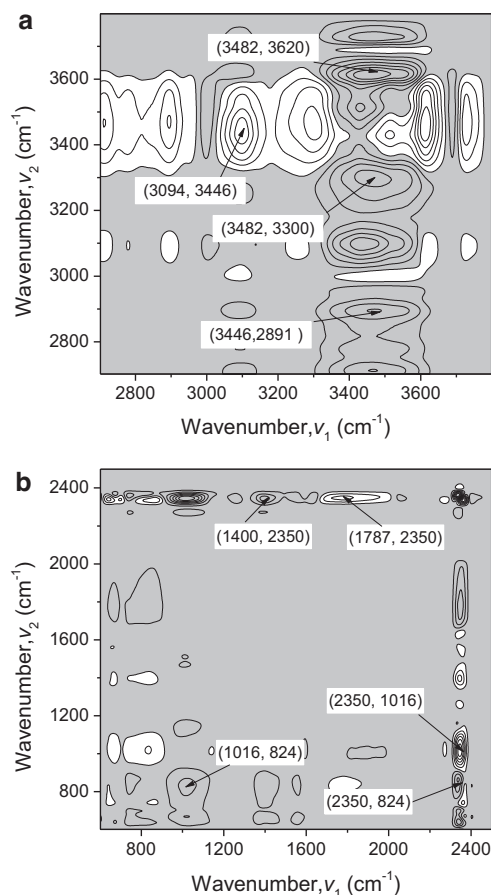


Fig. 4. Asynchronous two-dimensional correlation spectrum in 3800–2700 cm^{-1} (a) and 2500–600 cm^{-1} (b). White and gray areas refer to positive and negative intensities, respectively.

3446), positive $\Phi(3482, 3300)$ and negative $\Phi(3446, 2891)$, respectively (shown in Fig. 2a). According to Noda's rules, the change of primary amide $-\text{NH}_2$ at 3482 cm^{-1} mainly follows the change in $-\text{OH}$ group at 3620 cm^{-1} ; the change of secondary amide at 3094 cm^{-1} predominantly precedes the change in amines at 3446 cm^{-1} ; the change of primary amide $-\text{NH}_2$ follows the change in pyrrole at 3300 cm^{-1} ; the change of amines precedes the change in aldehyde at 2891 cm^{-1} .

The asynchronous two-dimensional correlation spectrum in 2500–600 cm^{-1} , shown in Fig. 4b, depicts five couples of asynchronous cross peaks: negative $\Psi(1400, 2350)$, positive $\Psi(1787, 2350)$, positive $\Psi(2350, 1016)$, negative $\Psi(2350, 824)$ and negative $\Psi(1016, 824)$. The synchronous correlation intensities at the same coordinate of the five asynchronous cross peaks are negative $\Phi(1400, 2350)$, positive $\Phi(1787, 2350)$, negative $\Phi(2350, 1016)$, positive $\Phi(2350, 824)$ and negative $\Phi(1016,$

824), respectively (shown in Fig. 2b). Based on Noda's rules, the five asynchronous cross peaks indicate that the changes of azo compound $\text{N}=\text{N}$ at 1400 cm^{-1} , $\text{C}=\text{O}$ group at 1787 cm^{-1} , aliphatic $\text{C}-\text{N}/\text{C}-\text{O}$ at 1016 cm^{-1} , and nitrate $\text{N}-\text{O}$ at 824 cm^{-1} occur predominantly before the change of CO_2 at 2350 cm^{-1} , and the change of aliphatic $\text{C}-\text{N}/\text{C}-\text{O}$ before the change of nitrate $\text{N}-\text{O}$.

3.4. Variation in relative intensities of peaks

Each of DRIFT spectrum was transformed into an absorption spectrum with the Kubelka–Munk method [24]. The Kubelka–Munk units can be used for computing the normalized peak intensity (I_x/I_{max}) at the characteristic wavenumber ($x \text{ cm}^{-1}$), and I_x/I_{max} is taken as the relative concentration of the functional group at $x \text{ cm}^{-1}$. Figure 5 shows the variation in relative intensities of the peaks in the two-dimensional correlation spectrum.

In the spectral region from 3800 cm^{-1} to 2700 cm^{-1} (shown in Fig. 5a and b), the relative concentration (I_x/I_{max}) of $-\text{OH}$, primary amide, amines and secondary amide groups all had a significant reduction, when the N_2 atmosphere was replaced partially by CO_2 at 30 $^\circ\text{C}$. It implies that all of $-\text{OH}$, primary amide, amines and secondary amide groups are CO_2 adsorption sites, and their adsorption mechanisms are shown in Fig. 3 [23]. During the CO_2 adsorption process, these functional groups can react with CO_2 and play the role of CO_2 capture. As the temperature increased to 120 $^\circ\text{C}$, the relative concentration of $-\text{OH}$ group was nearly unchanged, but primary amide and amines kept on declining. It suggests that with the increase of temperature, some $-\text{OH}$ groups have no ability to absorb CO_2 , but primary amide and amines still have this ability. When the temperature increased to 200 $^\circ\text{C}$, there was an obvious rise to all of $-\text{OH}$, primary amide and amines, and the relative concentration of $-\text{OH}$ group was almost recovered to the level of non-adsorption, but primary amide and amines are both lower than the level of non-adsorption. It indicates that $-\text{OH}$ group has a good regeneration performance, but some of primary amide and amines are deactivated during the regeneration. When the temperature is 60 $^\circ\text{C}$, the relative concentration of secondary amide continued to keep falling. However, compared with $-\text{OH}$, primary amide and amines, the secondary amide began to regenerate with the temperature increased to 120 $^\circ\text{C}$, and it also showed a good regeneration characteristic at 200 $^\circ\text{C}$.

In comparison with the four groups above, when N_2 atmosphere was replaced partially by CO_2 , the relative concentrations of pyrrole and aldehyde both have no obvious decrease, and almost kept unchanged. As the temperature increased to 120 $^\circ\text{C}$, the aldehyde group started to increase, and the pyrrole still unchanged. However, there was an obvious rise to the pyrrole at 200 $^\circ\text{C}$. It implies that the

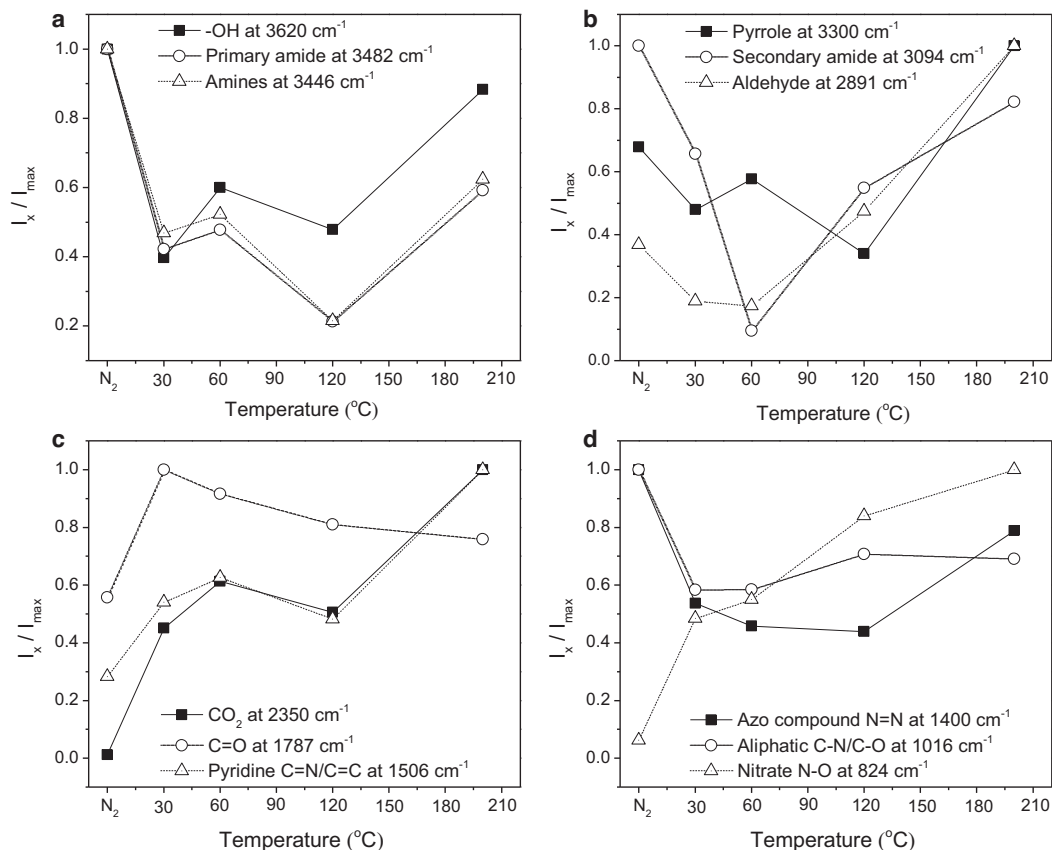


Fig. 5. Variation in relative intensities of peaks in the 2D perturbation correlation spectrum.

pyrrole and aldehyde groups both have little contribution to adsorb CO_2 . Conversely, they are the products of the adsorption and regeneration processes.

Figure 5c and d shows the variation in relative intensities of the peaks in 2500–600 cm^{-1} . When the N_2 atmosphere was replaced partially by CO_2 , pyridine $\text{C}=\text{N}/\text{C}=\text{C}$, $\text{C}=\text{O}$ and CO_2 obviously increased. With the increase of temperature, the relative concentration of $\text{C}=\text{O}$ groups decreased gradually, while pyridine $\text{C}=\text{N}/\text{C}=\text{C}$ and CO_2 almost kept unchanged before 120 $^\circ\text{C}$, and then increased greatly. It indicates that with the increase of temperature, $\text{C}=\text{O}$ groups decomposed gradually, and more pyridine $\text{C}=\text{N}/\text{C}=\text{C}$ groups were formed at the higher temperatures (over 120 $^\circ\text{C}$). The increase of CO_2 may be derived from the decomposition of $\text{C}=\text{O}$ groups and CO_2 desorption.

The azo compound $\text{N}=\text{N}$ and aliphatic $\text{C}-\text{N}/\text{C}-\text{O}$ groups also present the ability to adsorb carbon dioxide, when the N_2 atmosphere is converted to CO_2 . However, as the temperature increased to 120 $^\circ\text{C}$, their relative concentrations changed little. It implies that the increase of adsorption temperature has little effect on the

adsorption properties of azo compound $\text{N}=\text{N}$ and aliphatic $\text{C}-\text{N}/\text{C}-\text{O}$ groups. With the temperature increase to 200 $^\circ\text{C}$, aliphatic $\text{C}-\text{N}/\text{C}-\text{O}$ groups can hardly be regenerated, but azo compound $\text{N}=\text{N}$ group presents the regeneration performance.

4. Conclusions

The *in situ*-DRIFTS of 2D perturbation correlation method provides a reliable technique for online and real-time monitoring the interfacial reaction between adsorbent and adsorbate, and revealing mechanisms of CO_2 adsorption-desorption on the nitrogen enriched biochar. In CO_2 atmosphere, primary amide, secondary amide, aliphatic $\text{C}-\text{N}/\text{C}-\text{O}$ and nitrate $\text{N}-\text{O}$ groups most intensively respond to the external variable temperature. The hydroxyl, primary amide, amines, azo compound $\text{N}=\text{N}$ and secondary amide groups all present the ability to adsorb CO_2 , and most of them can be regenerated. The aliphatic $\text{C}-\text{N}/\text{C}-\text{O}$ also have the CO_2 adsorption performance, but can hardly be regenerated. Moreover, pyridine and nitrate $\text{N}-\text{O}$ groups are formed during both the adsorption and

regeneration processes, while pyrrole and aldehyde groups are only generated during the regeneration process.

Acknowledgment

The authors wish to express their sincere thanks to the financial support from the National Basic Research Program of China (2013CB228102), the National Natural Science Foundation of China (51276075 and 51506071), the Fundamental Research Funds for the Central Universities and the Special Fund for Agro-scientific Research in the Public Interest (201303095). The authors are also grateful for the technical support from Analytical and Testing Center in Huazhong University of Science & Technology.

References

- [1] J. Gibbins, H. Chalmers, *Energy Policy* 36 (2008) 4317–4322.
- [2] G.T. Rochelle, *Science* 325 (2009) 1652–1654.
- [3] C. Pevida, M. Plaza, B. Arias, J. Feroso, F. Rubiera, J. Pis, *Appl. Surf. Sci.* 254 (2008) 7165–7172.
- [4] D. Aaron, C. Tsouris, *Sep. Sci. Technol.* 40 (2005) 321–348.
- [5] S. Kazama, T. Teramoto, K. Haraya, *J. Membr. Sci.* 207 (2002) 91–104.
- [6] C.-H. Yu, C.-H. Huang, C.-S. Tan, *Aerosol Air Qual. Res.* 12 (2012) 745–769.
- [7] M.S. Shafeeyan, W.M.A.W. Daud, A. Houshmand, A. Shamiri, *J. Anal. Appl. Pyrolysis* 89 (2010) 143–151.
- [8] A. Heidari, H. Younesi, A. Rashidi, A.A. Ghoreyshi, *Chem. Eng. J.* 254 (2014) 503–513.
- [9] M.S. Shafeeyan, W.M.A.W. Daud, A. Houshmand, A. Arami Niya, *Appl. Surf. Sci.* 257 (2011) 3936–3942.
- [10] J. Przepiórski, M. Skrodzewicz, A.W. Morawski, *Appl. Surf. Sci.* 225 (2004) 235–242.
- [11] O. Ioannidou, A. Zabaniotou, *Renew. Sustain. Energy Rev.* 11 (2007) 1966–2005.
- [12] X. Zhang, S. Zhang, H. Yang, et al., *Energy* 91 (2015) 903–910.
- [13] W. Shen, W. Fan, *J. Mater. Chem. A* 1 (2013) 999–1013.
- [14] Y. Otake, R.G. Jenkins, *Carbon* 31 (1993) 109–121.
- [15] A.C. Chang, S.S. Chuang, M. Gray, Y. Soong, *Energy Fuels* 17 (2003) 468–473.
- [16] O.R. Harvey, B.E. Herbert, L.J. Kuo, P. Louchouart, *Environ. Sci. Technol.* 46 (2012) 10641–10650.
- [17] I. Noda, Y. Ozaki, *Two-dimensional Correlation Spectroscopy: Applications in Vibrational and Optical Spectroscopy*, John Wiley & Sons, New York, 2005.
- [18] I. Noda, *Appl. Spectrosc.* 47 (1993) 1329–1336.
- [19] X. Zhang, S. Zhang, H. Yang, et al., *Chem. Eng. J.* 257 (2014) 20–27.
- [20] M.A. Nahil, P.T. Williams, *Chem. Eng. J.* 184 (2012) 228–237.
- [21] R.J.J. Jansen, H. van Bekkum, *Carbon* 33 (1995) 1021–1027.
- [22] S. Biniak, G. Szymański, J. Siedlewski, A. Świątkowski, *Carbon* 35 (1997) 1799–1810.
- [23] A. Sayari, A. Heydari-Gorji, Y. Yang, *J. Am. Chem. Soc.* 134 (2012) 13834–13842.
- [24] M.P. Fuller, P.R. Griffiths, *Anal. Chem.* 50 (1978) 1906–1910.